



# Recombinant streptococcal protein G-modified metal-organic framework ZIF-8 for the highly selective purification of immunoglobulin G from human serum

Yufei Ma<sup>a,1</sup>, Yuhan Xiang<sup>a,1</sup>, Xin Li<sup>c,\*\*\*</sup>, Dandan Zhang<sup>b,\*\*</sup>, Qing Chen<sup>a,\*</sup>

<sup>a</sup> School of Pharmacy, Shenyang Medical College, Shenyang, 110034, People's Republic of China

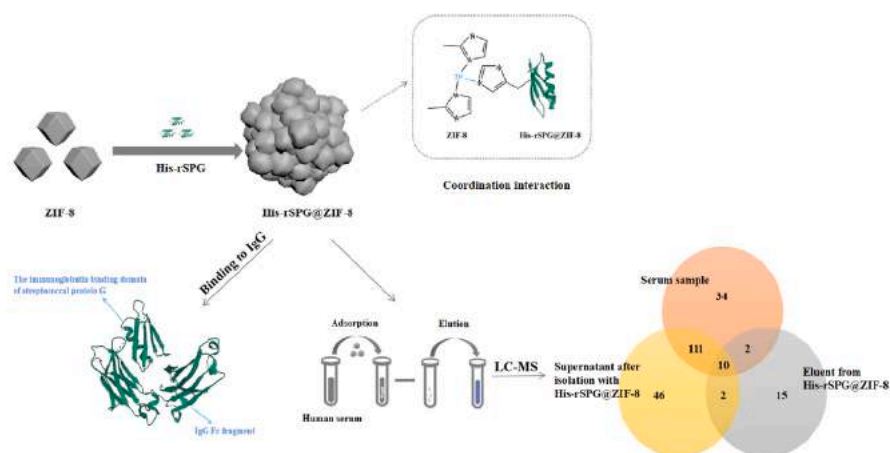
<sup>b</sup> School of Public Health, Shenyang Medical College, Shenyang, 110034, People's Republic of China

<sup>c</sup> Department of Science and Technology, Shenyang Medical College, Shenyang, 110034, People's Republic of China

## HIGHLIGHTS

- A novel solid phase extractant, His-rSPG@ZIF-8, was prepared by coordinating His-rSPG with ZIF-8.
- With rSPG's selectivity and ZIF-8's high surface area, His-rSPG@ZIF-8 shows excellent selectivity for IgG.
- A new method was constructed to isolate and identify IgG from human serum using His-rSPG@ZIF-8 as adsorbent.

## GRAPHICAL ABSTRACT



## ARTICLE INFO

**Keywords:**  
Metal-organic frameworks  
ZIF-8  
Immunoglobulin G  
Streptococcus protein G  
Separation/purification

## ABSTRACT

A novel solid phase extractant His-rSPG@ZIF-8 was prepared by covalently coupling recombinant streptococcal protein G (His-rSPG) with ZIF-8. The His-rSPG@ZIF-8 composite was characterized by Fourier transform infrared spectroscopy (FT-IR), Raman spectroscopy (Raman), X-ray photoelectron spectroscopy (XPS), scanning electron microscopy (SEM) and transmission electron microscopy (TEM). Due to the specific binding between the immunoglobulin binding region of His-rSPG and the Fc region of immunoglobulin G (IgG), the His-rSPG@ZIF-8 composite demonstrated exceptional selectivity in adsorbing IgG. In Britton-Robinson buffer (BR buffer) with a salt concentration of 500 mmol L<sup>-1</sup> (0.04 mol L<sup>-1</sup>, pH 8.0), the His-rSPG@ZIF-8 composite exhibited a

\* Corresponding author.

\*\* Corresponding author.

\*\*\* Corresponding author.

E-mail addresses: [htplixin@163.com](mailto:htplixin@163.com) (X. Li), [604859039@qq.com](mailto:604859039@qq.com) (D. Zhang), [chenqing.0906@163.com](mailto:chenqing.0906@163.com) (Q. Chen).

<sup>1</sup> Yufei Ma and Yuhan Xiang contributed equally to this work.

<https://doi.org/10.1016/j.aca.2023.342175>

Received 7 October 2023; Received in revised form 28 November 2023; Accepted 21 December 2023

Available online 25 December 2023

0003-2670/© 2023 Elsevier B.V. All rights reserved.

remarkable adsorption efficiency of 99.8 % for 0.05 mg of the composite on 200  $\mu\text{L}$  of IgG solution ( $100 \mu\text{g mL}^{-1}$ ). The adsorption behavior of the His-rSPG@ZIF-8 composite aligns with the Langmuir adsorption model, and the theoretical maximum adsorption capacity is  $1428.6 \text{ mg g}^{-1}$ . The adsorbed IgG molecules were successfully eluted using a SDS solution (0.5 %, m/m), resulting in a recovery rate of 91.2 %. Indeed, the His-rSPG@ZIF-8 composite was successfully utilized for the isolation and purification of IgG from human serum samples. The obtained IgG exhibited high purity, as confirmed by SDS-PAGE analysis. Additionally, LC-MS/MS analysis was employed to identify the human serum proteins following the adsorption and elution process using the His-rSPG@ZIF-8 composite material. The results revealed that the recovered solution contained an impressive content of immunoglobulin, accounting for 62.4 % of the total protein content. Furthermore, this process also led to the significant enrichment of low abundance proteins such as Serpin B4 and Cofilin-1. Consequently, the His-rSPG@ZIF-8 composite holds great promise for applications such as IgG purification and immunoassays. At the same time, it expands the application of metal-organic frameworks in the field of proteomics.

## 1. Introduction

Immunoglobulin G (IgG) is a crucial protein that plays a significant role in the immune system. It is primarily produced and secreted by B lymphocytes and widely recognized as the most prevalent immunoglobulin in serum [1]. IgG possesses several important functions, including enhancing the phagocytosis of bacteria and other particle antigens by phagocytic cells, activating the complement system, facilitating ADCC, and neutralizing toxins, among others [2,3]. It is worth noting that IgG is divided into four distinct subclasses: IgG1, IgG2, IgG3, and IgG4. Each subclass has different physiological functions and interacts with different IgG-Fc receptors (FC- $\gamma$ r) on immune cells [4]. Intravenous immunoglobulins (IVIg) can be used as a therapeutic treatment for primary immunodeficiency disorders and to prevent diseases like hypogammaglobulinemia, where there is a deficiency of IgG in the blood [5,6]. Recent studies have also discovered the presence of IgG in tumor cells. High levels of antibodies, including IgG, have been found to promote tumor cell proliferation. However, it has also been found that IgG produced by tumor cells can be blocked, leading to inhibition of tumor growth. Thus, tumor cell-derived IgG can be used as a potential therapeutic target [7]. In the field of proteomics, the separation and purification of IgG is also extremely important. By isolating and purifying IgG, its structure, function, and interactions with other proteins can be better understood. After the separation and purification of IgG, techniques such as mass spectrometry can be used to identify its protein components. This helps to discover disease biomarkers, which are protein molecules associated with certain diseases, providing important clues for early diagnosis and treatment of diseases [8]. Due to the crucial role of IgG in disease prevention, understanding disease mechanisms, and proteomics, purifying its monomeric form from complex samples is a major research focus.

Solid phase extraction (SPE) is an analytical method designed to separate the target analyte from the complex sample matrix, enabling its qualitative or quantitative determination [9]. It has emerged as an effective means of pretreatment of protein/polypeptide samples. The advancements in materials science have provided a wide range of adsorbents for protein separation and enrichment. These adsorbents can selectively separate and enrichment of specific proteins under controlled experimental conditions [10]. Currently, a wide range of solid-phase materials have been developed and utilized in various applications, such as magnetic nanoparticles, metal-organic frameworks, porous polymers and molecularly imprinted polymers [11–14]. Based on these materials, new methods for protein/peptide separation and enrichment have been established. For example, magnetic nanoparticles modified with nickel (Ni-MNPs) have a higher affinity for His labeled proteins and can obtain higher purity target proteins from complex sample matrices, such as silkworm expression system [15]. In addition,  $\beta$ -amyloid peptide ( $\text{A}\beta_{1-42}$ ) coupled to magnetic nanoparticles modified with PEI ( $\text{A}\beta_{1-42}$ @MNP) showed good adsorption for ovalbumin. Using  $\text{A}\beta_{1-42}$ @MNP as an adsorbent, ovalbumin with high abundance can be successfully removed from egg white samples, and this method also shows great ability in separating and identifying glycoproteins in egg

white [16].

Metal-organic frameworks (MOFs) are a rapidly developing class of organic-inorganic hybrid material. They consist of metal ions/ion clusters supported by organic ligands and coordinated by these ligands [17]. MOFs possess several advantages, including high specific surface area, adjustable pore size, diverse structural composition, open metal sites, and the ability for chemical modification [18], and are widely used in catalysis, sensing, adsorption and ion exchange [19–22]. For instance, zirconia-based MOFs (Zr-MOFs) can be assembled with fluorescent DNA through Zr-O-P bonds. This assembly can be utilized as functional probe-quencher pairs, enabling the establishment of molecular sensing and logic systems [23]. ZIF-8, a type of MOFs, is an innovative nanoporous material with a zeolite topology, composed of Zn ions and 2-methylimidazole [24]. It stands out due to its remarkable features, including a large specific surface area, uniform pore size, and high thermal stability [25]. These characteristics make ZIF-8 an excellent candidate for applications as a stationary phase in separation techniques. For instance, the layer-by-layer preparation of Terpolymer@ZIF-8 through by free radical polymerization, followed by surface modification with aminophenylboric acid (AMBA), enables the successful separation of mono- and multi-glycosylated peptides using the resulting Terpolymer@ZIF-8@BA composite [26]. Additionally, ZIF-8 can be combined with other materials to create functional composite materials that find wide applications, in gas storage, catalysis and other fields [27,28]. Furthermore, ZIF-8 exhibits strong biocompatibility, making it highly suitable for drug delivery applications [29]. For example, the combination of ZIF-8 with Celecoxib can develop a pH-responsive, multi-function intelligent drug delivery system known as CEL@ZIF-8 [30]. This enhanced drug delivery system offers multiple functions, including antibacterial, osteogenic, anti-inflammatory and intelligent release. It holds great potential for clinical application prospects in the treatment of chronic osteomyelitis.

Streptococcal protein G (SPG) is a naturally occurring protein derived from microbes. It is typically isolated independently from streptococcus bacteria and has the special ability to bind reversibly to the Fc region of most mammalian immunoglobulins through a highly effective binding mechanism [31]. Due to this reversible mechanism, SPG exhibits high selectivity towards immunoglobulins, making it suitable for the isolation and purification of IgG. In most cases, recombinant Streptococcal protein G (rSPG) is preferred over natural SPG. The amino acid sequence of SPG whole protein can be divided into four main parts: N-terminal signal peptide region, the albumin binding region AB, the immunoglobulin binding region CD and the C-terminal protein anchor region. The CD region primarily interacts with Fc fragments of IgG. Within the CD region, there are three individual domains (C1, C2, and C3) separated by interval domains D1 and D2, which have identical sequences. These two intervals have the same sequence. Each domain of the CD region is capable of binding to Fc fragments of IgG [32,33]. rSPG removes the albumin-binding region and protein-anchored region, retaining only retains the immunoglobulin binding region. As a result, rSPG exhibits a stronger binding ability to IgG [34]. Although recombinant Staphylococcal Protein A (rSPA) can also bind to IgG, rSPG has its

unique advantages. rSPG exhibits high affinity for IgG, enabling the selective binding and purification of IgG. This high affinity allows rSPG to demonstrate greater selectivity and efficiency in purifying target proteins. Additionally, it can bind to IgG from various mammalian and some non-mammalian sources, including humans, mice, rabbits, and others. This expands its applicability to samples from diverse origins. Furthermore, rSPG demonstrates excellent thermal stability and chemical stability, maintaining its structural and functional integrity under different experimental conditions [35].

Affinity chromatography is commonly used for antibody purification, with rSPG being a widely used affinity ligand. However, prior to purifying antibodies through affinity chromatography, salt precipitation is required as a primary purification step, which can be cumbersome, time-consuming, and result in significant sample loss [36]. Therefore, it is necessary to choose a simple and efficient method for antibody purification. SPE is a better choice as it only requires a single step for antibody enrichment, making it both simple and efficient. Considering the various advantages of ZIF-8, this study selected it as the suitable SPE material.

In this study, we developed a new bioconjugated nanoparticle called His-rSPG@ZIF-8 by connecting rSPG with a histidine tag (His-rSPG) to ZIF-8 nanoparticles through coordination interaction. By leveraging the strong selectivity of rSPG for IgG and the high specific surface area of ZIF-8, this composite demonstrates excellent adsorption selectivity for IgG as a solid phase extractant. Consequently, we have successfully developed a novel composite consisting of recombinant protein and metal-organic framework (His-rSPG@ZIF-8) for the purification of human serum IgG. This achievement not only demonstrates the potential of MOFs in the field of life science but also expands their application in protein purification.

## 2. Experimental

### 2.1. Materials and reagents

IgG, human serum albumin (HSA) and transferrin (Trf) were obtained from Sigma-Aldrich (St. Louis, USA). His-rSPG was obtained from Beyotime Biotechnology (Shanghai, China).  $\text{Zn}(\text{NO}_3)_2 \cdot 6\text{H}_2\text{O}$ ,  $\text{H}_3\text{PO}_4$ ,  $\text{H}_3\text{BO}_3$ , NaCl, HCl, 2-methylimidazole (2-MIM), ethanol, acetic acid, tris (hydroxymethyl) aminomethane (Tris), and sodium dodecyl sulfate (SDS) were purchased from Sinopharm Chemical Reagent Co. Ltd. (Shanghai, China). The protein molecular weight marker used in our experiments (Broad, 3597A, Takara Biotechnology Co., LTD., Dalian, China) consists of eight purified proteins (myosin protein, Mr 200 kDa;  $\beta$ -galactosidase, Mr 116 kDa; Phosphorylase b, Mr 97.2 kDa; Serum albumin, Mr 66.4 kDa; Ovalbumin, Mr 44.3 kDa; Carbonic anhydrase, Mr 29.0 kDa; Trypsin inhibitor, Mr 20.1 kDa; Lysozyme, Mr 14.3 kDa). All experiments were conducted using 18 M $\Omega$  cm of deionized water (ddH<sub>2</sub>O).

### 2.2. Instrumentation

FT-IR spectra were acquired using a Nicolet 6700 with wavenumbers ranging from 400 to 4000  $\text{cm}^{-1}$  (Thermo Fisher Nicolet, USA). Raman spectra were obtained on Renishaw inVia Raman spectrometer (Renishaw, Britain). SEM images were captured using a Hitachi SU8020 scanning electron microscope (Hitachi, Japan), and energy X-ray dispersive (EDS) analysis was performed using a HORIBA EX350 (HORIBA Scientific, Ltd., France). N<sub>2</sub> adsorption-desorption isotherm was measured by ASAP 2020HD88 BET analyzer. TEM images were taken on HITACHI H7650 transmission electron microscope (Hitachi, Japan). X-ray photoelectron spectroscopy (XPS) was conducted using the ESCALAB 250Xi Surface analysis system. LC-MS/MS analysis was performed using an Easy nano-LC 1000 system (Thermo Fisher Scientific, Germany) interfaced with a Q Exactive Orbitrap mass spectrometer (Thermo Fisher Scientific, Germany). The Swiss-Prot database filtered

for Homo sapiens taxonomy was utilized for data analysis and identification.

### 2.3. Synthesis of the His-rSPG@ZIF-8 composite

To prepare a concentrated storage solution, 5 mg His-rSPG was added to 1 mL of ddH<sub>2</sub>O, resulting in a concentration of 5  $\text{mg mL}^{-1}$ . Then, 100  $\mu\text{L}$  of the protein concentrated storage solution was absorbed into a centrifuge tube and diluted by adding 2.4 mL of ddH<sub>2</sub>O, yielding a final protein solution with a concentration of 200  $\mu\text{g mL}^{-1}$ . This solution was refrigerated for future use. 2 mg ZIF-8 powder was dispersed in ddH<sub>2</sub>O by ultrasound until it was uniformly dispersed. The dispersion was then centrifuged at 8000 rpm for 5 min, and the supernatant was discarded. 2 mL of the previously prepared His-rSPG solution (200  $\mu\text{g mL}^{-1}$ ) was added to the centrifuge tube containing the processed ZIF-8. After thorough shaking for 2 h, the mixture was centrifuged at 6000 rpm for 5 min, and the supernatant was discarded. The resulting product was washed with water for 2-3 times. Finally, the product was freeze-dried and preserved.

### 2.4. Adsorption/desorption of proteins by His-rSPG@ZIF-8 composite

The adsorption behavior of different protein models, including IgG, HSA and Trf, on the His-rSPG@ZIF-8 composite was investigated. The acidity of protein solutions was controlled by BR buffer with the pH range of 6.0–10.0.

The procedure is as follows: Add 0.05 mg His-rSPG@ZIF-8 composite to a 500  $\mu\text{L}$  centrifuge tube. Mix it 200  $\mu\text{L}$  100  $\mu\text{g mL}^{-1}$  protein solution. Shake the mixture for 15 min to facilitate adsorption. Centrifuge the tube at 6000 rpm for 5 min to separate the His-rSPG@ZIF-8 composite from the solution. After separation, 60  $\mu\text{L}$  supernatant was collected and 300  $\mu\text{L}$  Coomassil brilliant blue G250 solution was added. The residual protein concentration in the solution was quantified by measuring the absorption peak intensity of protein solution at 595 nm after staining. The concentration of protein before and after adsorption was calculated using the standard working curve. The adsorption efficiency of protein in the experiment was calculated by equation (1):  $C_0$  represents the concentration of original protein and  $C_1$  represents the concentration of residual protein after adsorption.

$$E_1 = \frac{C_0 - C_1}{C_0} \times 100\% \quad (1)$$

After the adsorption process, the His-rSPG@ZIF-8 composite was collected. To promote the recovery of the adsorbed protein on the surface of the His-rSPG@ZIF-8 composite, 200  $\mu\text{L}$  SDS solution (0.5%, m/m) was added and shaken for 20 min. After shaking, the mixture was centrifuged at 6000 rpm for 5 min. The supernatant was collected for assessment of elution efficiency or follow-up studies.

### 2.5. Isolation of IgG from healthy human serum

Serum samples were diluted 500 times with a neutral salt concentration of 0.5  $\text{mol L}^{-1}$  BR buffer (0.04  $\text{mol L}^{-1}$ , pH 8.0). 0.2 mg His-rSPG@ZIF-8 composite was mixed with 200  $\mu\text{L}$  of the diluted serum, fully shaken for 15 min, and centrifuged at 6000 rpm for 5 min. Serum before and after adsorption by His-rSPG@ZIF-8 composite was collected. Then, the His-rSPG@ZIF-8 composite after adsorbed protein was pre-washed with ddH<sub>2</sub>O and PBS buffer (0.01  $\text{mol L}^{-1}$ , pH 7.2), and the adsorbed protein was recovered with SDS solution (0.5%, m/m) as eluent. Finally, the supernatant and eluent were analyzed by polyacrylamide gel electrophoresis (SDS-PAGE).

### 3. Results and discussion

#### 3.1. Characterization of the His-rSPG@ZIF-8 composite

ZIF-8 is a porous material composed of zinc ions and 2-MIM, where the surface contains coordination unsaturated Zn ions that can interact with histidine-rich proteins to form complexes. Taking advantage of this, a recombinant protein-metal-organic framework composite was prepared by coordinating the His tag on the His-rSPG protein with the Zn ions present in ZIF-8. This coordination interaction allows for the formation of stable complexes between the recombinant protein and the metal-organic framework (Scheme 1).

We optimized the material synthesis in the preliminary experiment. After coordinating 2 mg of ZIF-8 with different concentrations of His-rSPG, the synthesized composite was used for the purification of IgG. As shown in Fig. S1, when the concentration of His-rSPG was 200  $\mu\text{g mL}^{-1}$ , the adsorption efficiency of IgG by the composite reached equilibrium. This is because at a concentration of 200  $\mu\text{g mL}^{-1}$ , the unsaturated Zn ions on the surface of ZIF-8 reached saturation, so the adsorption efficiency of IgG was not affected even with an increase in the concentration of the recombinant protein. Therefore, a concentration of 200  $\mu\text{g mL}^{-1}$  of His-rSPG was ultimately selected for the experiment.

The composition, structure, and properties of the His-rSPG@ZIF-8 composite were characterized by FT-IR, Raman, XPS, EDS, BET, SEM, and TEM, which demonstrated the successful synthesis of the His-rSPG@ZIF-8 composite.

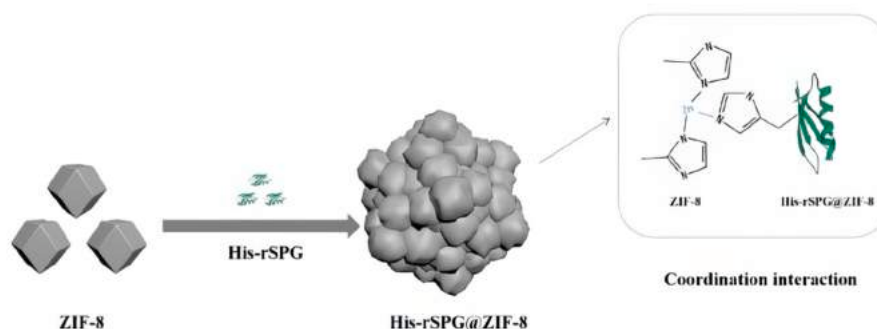
Fig. 1A is the infrared spectrum of ZIF-8, rSPG, His-rSPG@ZIF-8 composite. In the FT-IR of ZIF-8, the bands at 3166  $\text{cm}^{-1}$  are the stretching vibrations of aromatic C-H groups in imidazole groups, and the bands at 2931  $\text{cm}^{-1}$  and 2838  $\text{cm}^{-1}$  are the stretching vibrations of aliphatic C-H groups [37]. The bands at 1579  $\text{cm}^{-1}$  and 422  $\text{cm}^{-1}$  belong to C=N stretching vibration and Zn-N stretching vibration, respectively. The characteristic peaks at 995  $\text{cm}^{-1}$  and 1145  $\text{cm}^{-1}$  are attributed to C-N stretching vibration [38]. In the infrared spectrum of His-rSPG, a large and wide absorption peak can be seen at 3000–3500  $\text{cm}^{-1}$ , which is attributed to the stretching vibrations of O-H and N-H in the protein [39]. Meanwhile, asymmetric stretching vibration belonging to -COOH and symmetric stretching vibration belonging to -COOH appeared at 1602  $\text{cm}^{-1}$  and 1359  $\text{cm}^{-1}$  respectively [40]. Due to the small molecular weight of the His tag compared to the entire protein, the infrared peak corresponding to the characteristic peak of the imidazole ring in the His tag is not prominently observed in the spectrum of the recombinant protein. However, in the infrared spectrum of the His-rSPG@ZIF-8 composite, a significant enhancement in the C-N stretching vibration at 1045  $\text{cm}^{-1}$  is observed. This enhancement can be attributed to the  $\pi$ - $\pi$  stacking interaction between the imidazole ring present in ZIF-8 and the imidazole ring of the His tag, present in the His-rSPG protein [41]. Furthermore, the characteristic peaks associated with proteins appeared around 1608  $\text{cm}^{-1}$ , 1365  $\text{cm}^{-1}$ , and in the range of 3000–3500  $\text{cm}^{-1}$ . These peaks indicate the presence of protein components in the

composite material, further confirming the successful combination of His-rSPG with ZIF-8 to form a new composite.

Fig. 1B shows the Raman spectra of ZIF-8 and His-rSPG@ZIF-8 composite. In the Raman spectrum of ZIF-8, the characteristic peaks observed at 175  $\text{cm}^{-1}$ , 1144  $\text{cm}^{-1}$  and 1462  $\text{cm}^{-1}$  correspond to the vibrations of Zn-N stretching, C5-N stretching and methyl bending, respectively [42]. Raman spectra of His-rSPG@ZIF-8 composite show that the characteristic peaks at 477  $\text{cm}^{-1}$  and 593  $\text{cm}^{-1}$  are attributable to the out-of-plane deformation vibrations of imidazole rings and the symmetric deformation vibrations of  $\text{NH}_2$  of proteins. The strong peak observed at 980  $\text{cm}^{-1}$  in the Raman spectrum of the His-rSPG@ZIF-8 composite is attributed to the in-plane respiratory vibration of the imidazole ring. This strong peak is a result of the  $\pi$ - $\pi$  stacking interaction between the imidazole ring of the His tag and the imidazole ring in ZIF-8 [43]. In contrast, the peak observed at this position in the Raman spectrum of ZIF-8 is very weak. This is because the in-plane respiratory vibration peaks of the imidazole ring in the His-rSPG@ZIF-8 composite are much stronger, which can overshadow and mask the weaker peaks.

Fig. 1C shows the EDS spectra of His-rSPG@ZIF-8 composite. The results obtained from the characterization techniques indicate that the His-rSPG@ZIF-8 composite contains not only the C, N, and Zn elements present in ZIF-8 but also the O element, which is characteristic of proteins. This presence of the O element further confirms the successful synthesis of the His-rSPG@ZIF-8 composite. The atomic percentages of C, N, Zn and O in the composite were 12.9 %, 6.1 %, 6.3 % and 74.7 %, respectively. Fig. S2 shows the  $\text{N}_2$  adsorption-desorption isotherm of ZIF-8 at 196  $^\circ\text{C}$ . The total adsorption capacity of ZIF-8 is consistent with the literature report [44]. Table S1 lists the specific surface area and average pore size of ZIF-8, which are confirmed to be 1447.4  $\text{m}^2\text{g}^{-1}$  and 2.3 nm, respectively, demonstrating a high specific surface area of ZIF-8.

Fig. 1D–F The chemical structure of the material was characterized by XPS. Fig. 1D is the energy spectrum of Zn 2p XPS of ZIF-8 and His-rSPG@ZIF-8 composite. It can be seen that the signal peaks of Zn 2p<sub>3/2</sub> and Zn 2p<sub>1/2</sub> in ZIF-8 appear at 1021.1 eV and 1044.2 eV, respectively. The signal peak position of Zn 2p<sub>3/2</sub> and Zn 2p<sub>1/2</sub> of His-rSPG@ZIF-8 composite at 1021 eV and 1044.1 eV, respectively, are observed to be lower than those of ZIF-8. This slight decrease in energy is attributed to the subtle difference in the Zn-N coordination between Zn-His and Zn-MIM in the composite. As a result, it leads to an increase in the electron cloud density at the Zn site in the His-rSPG@ZIF-8 composite [45]. Fig. 1E shows the C 1s XPS spectra of ZIF-8 and His-rSPG@ZIF-8 composite. The signal peaks at 284.8 eV and 285.8 eV correspond to the C-C and C-N bonds, respectively. In the His-rSPG@ZIF-8 composite, a new signal peak at 288.2 eV emerges, which can be attributed to the O=C-NH functional group of the protein [46]. In Fig. 1F, the O 1s XPS spectrum of His-rSPG@ZIF-8 composite was presented. Interestingly, a signal peak at 531.3 eV corresponding to O=C is observed, indicating the presence of protein in the composite. This observation confirms the successful binding of the recombinant protein with ZIF-8 in the composite.



Scheme 1. Schematic of the preparation of His-rSPG@ZIF-8 composite by the coordination interaction between His-rSPG and ZIF-8.

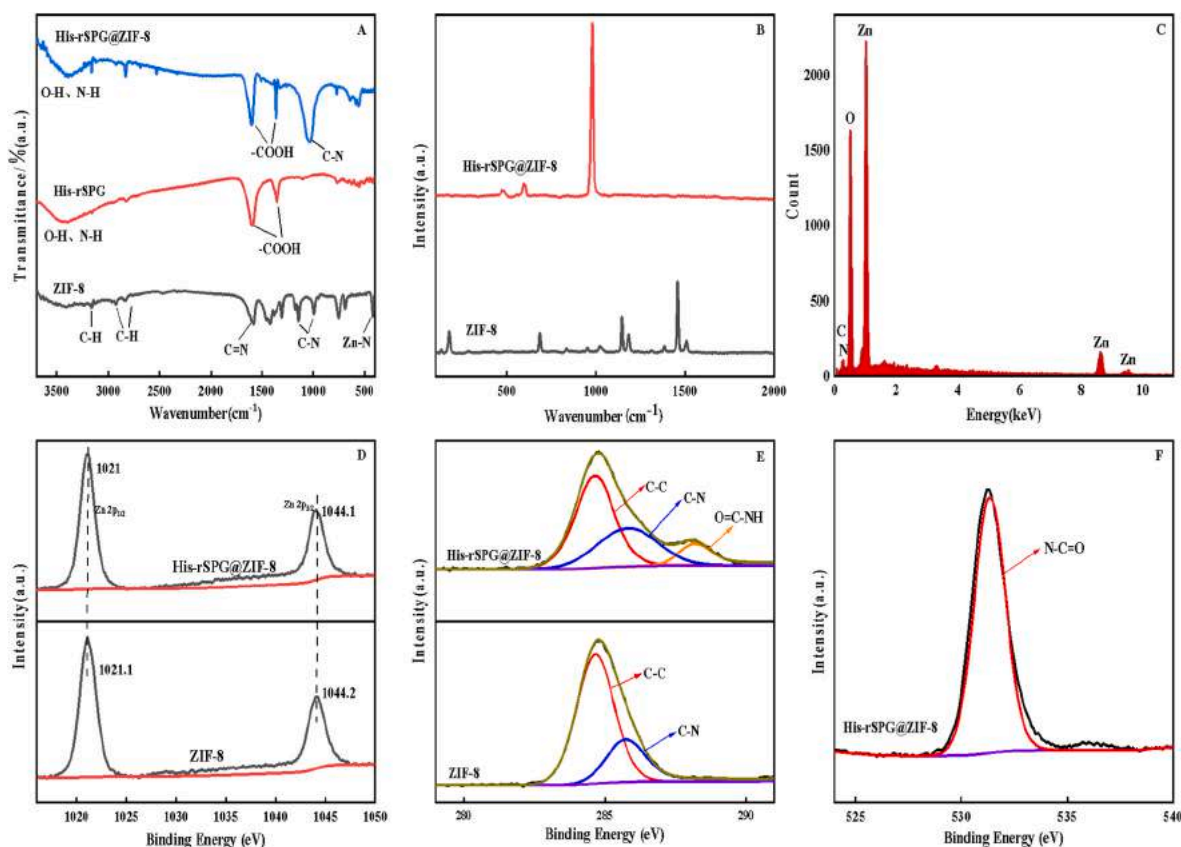


Fig. 1. FT-IR spectra of ZIF-8, His-rSPG and His-rSPG@ZIF-8 (A). Raman spectra of ZIF-8 and His-rSPG@ZIF-8 (B). EDS spectra (C) of His-rSPG@ZIF-8. High-resolution Zn 2p (D), C 1s (E), and O 1s (F) XPS spectra of ZIF-8 and His-rSPG@ZIF-8.

Fig. 2A and C depict SEM images of ZIF-8 and the His-rSPG@ZIF-8 composite, respectively. In Fig. 2A, ZIF-8 exhibits a clear surface profile with a smooth texture and an average particle size of approximately 200 nm. However, as demonstrated in Fig. 2C, upon the addition of His-rSPG through coordination, the surface of the resulting His-rSPG@ZIF-8

composite no longer appears smooth, and the contour becomes less distinct. Additionally, noticeable aggregation phenomena are observed, leading to an increase in the average particle size to around 500 nm. Fig. 2B and D exhibit TEM images of ZIF-8 and the His-rSPG@ZIF-8 composite, respectively. In Fig. 2B, ZIF-8 is observed as a nanoparticle with a well-defined outline and a smooth surface, aligning with the SEM images. However, upon binding to His-rSPG, the surface of the ZIF-8 particles becomes uneven, accompanied by aggregation, as depicted in Fig. 2D. These results collectively suggest the successful synthesis of the His-rSPG@ZIF-8 composite.

### 3.2. Adsorption of proteins by His-rSPG@ZIF-8 composite

Three high abundance proteins in serum, IgG, HSA and Trf, were used as model proteins to study the adsorption ability of His-rSPG@ZIF-8 composite to proteins. Their isoelectric points (pI) were 8.0, 4.9 and 5.9, respectively. In this experiment, the adsorption of these three proteins by the His-rSPG@ZIF-8 composite was investigated in the pH range of 5.0–10.0. As shown in Fig. 3A, the highest adsorption efficiency observed was 91.2 % at pH 8.0. Within the pH range of 5–8, the adsorption efficiency of IgG exhibited a gradual increase with rising pH, followed by a decrease beyond pH 8.0. For both HSA and Trf, the adsorption efficiency was around 20 % to 30 %. Therefore, pH 8.0 was chosen as the optimal adsorption pH in this experiment. Meanwhile, the adsorption of these three proteins by ZIF-8 was conducted at pH 7.0–10.0, as ZIF-8 displays instability at pH levels below 6. The results shown in Fig. 3B showed that without modification of the recombinant protein, the adsorption efficiency of IgG by ZIF-8 was approximately 60 %. For HSA and Trf, the adsorption efficiency was essentially identical to that of the composite, suggesting that the adsorption of HSA and Trf by the composite was due to non-specific adsorption of ZIF-8.

rSPG has three IgG-binding domains that are capable of binding to

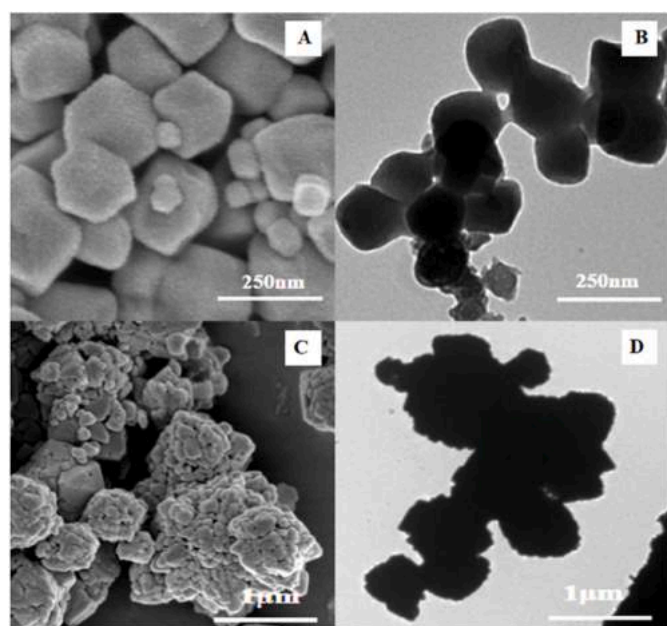
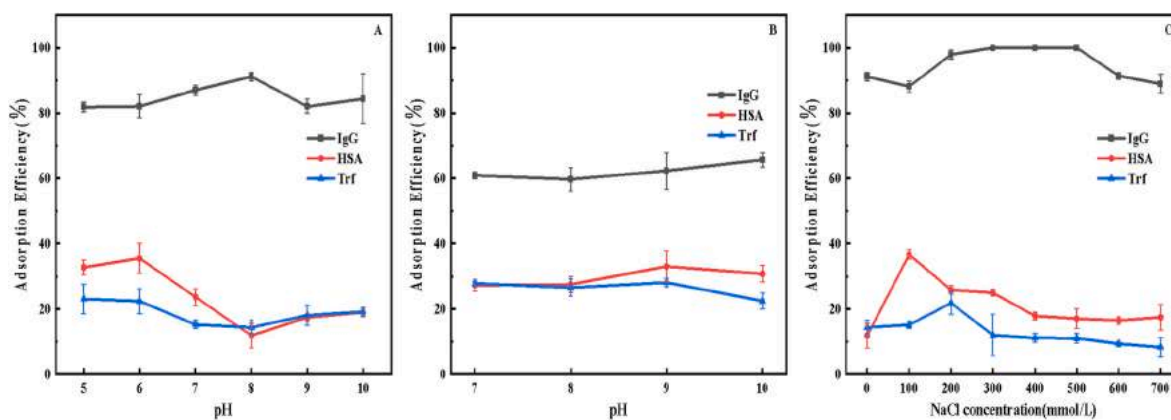


Fig. 2. SEM images of ZIF-8 and His-rSPG@ZIF-8 (A, C) and TEM images of ZIF-8 and His-rSPG@ZIF-8 (B, D).



**Fig. 3.** pH-dependent adsorption behaviors of IgG, HSA and Trf onto His-rSPG@ZIF-8 surface (A). pH-dependent adsorption behaviors of IgG, HSA and Trf onto ZIF-8 surface (B). Effect of the ionic strength of the adsorption efficiency of IgG, HSA and Trf (C). Protein solution: 100  $\mu\text{g mL}^{-1}$ , 200  $\mu\text{L}$ ; His-rSPG@ZIF-8: 0.05 mg.

the Fc fragment of IgG. The binding mechanism is closely associated with the secondary and tertiary structure of the rSPG recombinant protein. The protein docking between the rSPG IgG-binding domain and the IgG Fc fragment is visually represented in Fig. S3, illustrating a schematic diagram of the interaction. The IgG binding domain of rSPG consists of four  $\beta$  chains arranged around a central  $\alpha$ -helix segment. Among these, the amino acid residues located on the  $\alpha$ -helix play a crucial role in maintaining a stable binding state with the Fc fragment of IgG and contribute to the formation of the majority of stable hydrogen bonds. In addition, rSPG possesses two hydrophobic amino acid residues (ALA23 and ALA24), which can interact with the hydrophobic amino acid residues (MET-252, ILE-253, etc.) on the IgG Fc fragment, forming hydrophobic bonds [47,48]. Consequently, the adsorption of IgG by the His-rSPG@ZIF-8 composite is primarily driven by hydrogen bonding and hydrophobic interactions. Leveraging the impressive specific surface area and favorable biocompatibility of ZIF-8, the His-rSPG@ZIF-8 composite enables high selectivity, remarkable capacity, and efficient separation and analysis of IgG. The decrease in pH led to the protonation of the imidazole nitrogen atom in histidine and the consequent disruption of the coordination bond between histidine and the transition metal. As a result, the adsorption capability was compromised at pH levels below 8.0. At pH values greater than 8.0, the surface of IgG (pI 8.0) becomes negatively charged, while the material's surface is also negatively charged due to the modification of rSPG (pI 4.79). Therefore, with the increase of pH, the electrostatic repulsion between IgG and His-rSPG@ZIF-8 composite becomes obvious, which in turn reduces the adsorption efficiency of IgG. However, the adsorption efficiency also reached about 80 %, indicating that electrostatic interaction was not the main force between IgG and the composite. For HSA (pI 4.9) and Trf (pI 5.9), the electrostatic repulsion increased with increasing pH, resulting in a slight decrease in adsorption efficiency.

The influence of solution ionic strength of the solution on the protein adsorption behavior depicted in Fig. 3C, where we manipulated the ionic strength of the solution by adding varying amounts of NaCl to the protein solution at pH 8.0. For IgG, HSA and Trf, the adsorption efficiency initially increased and then decreased with the increase of salt concentration. For IgG, the adsorption efficiency of IgG increased in the range of salt concentration from 0 to 500  $\text{mmol L}^{-1}$ , and the adsorption efficiency was close to 100 %. As the salt concentration continued to increase, the adsorption efficiency of His-rSPG@ZIF-8 composite for IgG decreased. For HSA and Trf, the adsorption efficiency increased first and then decreased with the increase of salt concentration. The initial increase in adsorption efficiency can be attributed to the exposure of hydrophobic regions on the protein surface caused by an optimal concentration of neutral salts, enhancing the protein's hydrophobicity and promoting higher adsorption efficiency. With further increased in salt concentration, the competition between salt molecules and protein

molecules became more intense, resulting in a decrease in adsorption efficiency. However, even with this effect, the composite still achieved an IgG adsorption efficiency of over 85 % within the NaCl concentration range of 0–700  $\text{mmol L}^{-1}$ . This suggests that hydrogen bonding is the primary driving force for the composite's adsorption of IgG. Considering that the low ionic strength would be beneficial for the subsequent studies, BR buffer (0.04  $\text{mol L}^{-1}$ , pH 8.0) with a salt concentration of 500  $\text{mmol L}^{-1}$  was selected as the protein solvent in the experiment.

The effect of adsorption time on IgG adsorption efficiency was shown in Fig. S4A, illustrating that the adsorption efficiency of IgG gradually increased with the duration of time, ranging from 0 to 25 min. At an adsorption time of 15 min, the IgG adsorption efficiency reached approximately 100 %. After this point, the adsorption process tend to reach equilibrium. Thus, based on these results, we determined that 15 min was the optimal adsorption time for IgG in this study. We also explored the impact of adsorption temperature on IgG adsorption efficiency. As depicted in Fig. S4B, the His-rSPG@ZIF-8 composite exhibited an IgG adsorption efficiency of over 90 % within the temperature range of 5–25  $^{\circ}\text{C}$ . Moreover, the adsorption efficiency approaches 100 % when the temperature surpasses 15  $^{\circ}\text{C}$ . Taking all factors into consideration, we have determined that room temperature, approximately 20  $^{\circ}\text{C}$ , was the optimal adsorption temperature for our study.

To evaluate the adsorption capacity of His-rSPG@ZIF-8 composite for IgG, its ability to adsorb IgG at different concentrations (100–600  $\mu\text{g mL}^{-1}$ ) was investigated under a salt concentration of 500  $\text{mmol L}^{-1}$  and pH 8.0. The results are shown in Fig. 4A, where the unit adsorption of IgG by the His-rSPG@ZIF-8 composite gradually increased as the concentration of IgG increased. When the concentration of IgG was greater than 400  $\mu\text{g mL}^{-1}$ , the unit adsorption capacity of the His-rSPG@ZIF-8 composite for IgG remained stable, indicating that the adsorption capacity was basically saturated. It can be seen from the above that the adsorption of IgG on the surface of the His-rSPG@ZIF-8 composite is a monolayer adsorption, and the experimental data are in accordance with the Langmuir model. The formula is (2):

$$Q^* = \frac{Q_m \times C_e}{K_d + C_e} \quad (2)$$

where  $C_e$  is the equilibrium concentration of IgG ( $\text{mg L}^{-1}$ ),  $Q^*(q_{\text{eq}})$  is the equilibrium adsorption capacity ( $\text{mg g}^{-1}$ ),  $Q_m$  is the maximum adsorption capacity ( $\text{mg g}^{-1}$ ), and  $K_d$  is the adsorption equilibrium constant. As shown in Fig. S5, a linear relationship was observed between  $1/q_{\text{eq}}$  and  $1/C_e$ , with a linear equation of  $1/q_{\text{eq}} = 0.00185C_e + 0.0007$  and a correlation coefficient of  $R^2 = 0.992$ , indicating a good correlation between the adsorption behavior of His-rSPG@ZIF-8 composite for IgG and the Langmuir isotherm model. Based on this, it can be inferred that the adsorption of IgG by the material is a monolayer adsorption. The theoretical maximum adsorption capacity ( $Q_m$ ) was

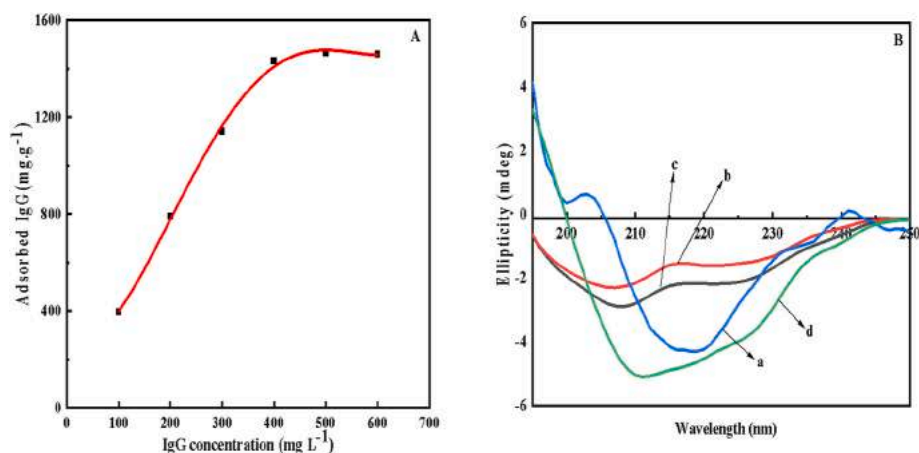


**Fig. 4.** The adsorption isotherm of IgG on the His-rSPG@ZIF-8 composite (A). Protein solution: 100–600  $\mu\text{g mL}^{-1}$ , 200  $\mu\text{L}$ ; His-rSPG@ZIF-8: 0.05 mg. Soret region CD spectra of IgG (B). 100  $\mu\text{g mL}^{-1}$  IgG in deionized water (a); IgG stripped into SDS solution (0.5%, m/m) as eluate (b); IgG directly dissolved in SDS solution (0.5%, m/m) (c); IgG in the eluate after removal of SDS by use of ultrafiltration (d).

calculated to be 1428.6  $\text{mg g}^{-1}$  from the intercept of the straight line in Fig. S5. Table 1 presents a comparison of the IgG adsorption capacities between other reported materials and the His-rSPG@ZIF-8 composite. It is evident that the His-rSPG@ZIF-8 composite exhibits significantly superior adsorption capacity compared to the other materials, highlighting its notable advantages in this regard.

Additionally, the adsorption selectivity and adsorption capacity of recombinant staphylococcal protein A (His-rSPA) modified ZIF-8 on IgG were compared. Fig. S6A investigated the effect of pH (5.0–10.0) on the adsorption efficiency of IgG and HSA by His-rSPA@ZIF-8 composite. For IgG, the highest adsorption efficiency was observed at pH 8.0, reaching 68.9%. It is significantly lower than that of His-rSPG@ZIF-8 composite. In addition, Fig. S6B examined the adsorption capacity of His-rSPA@ZIF-8 composite for different concentrations of IgG. Under the same pH value and ionic strength as His-rSPG@ZIF-8 composite, the adsorption capacity was evaluated, and the results showed that the theoretical maximum adsorption capacity was 1111.1  $\text{mg g}^{-1}$ , much lower than that of His-rSPG@ZIF-8 composite.

In order to effectively recover IgG adsorbed on the surface of His-rSPG@ZIF-8 composite, a series of eluents were investigated for IgG elution performance, such as NaCl (3  $\text{mol L}^{-1}$ ), ddH<sub>2</sub>O, PBS (0.01  $\text{mol L}^{-1}$ , pH 7.2), imidazole (50  $\text{mmol L}^{-1}$ ), and SDS (0.5%, m/m). The results depicted in Fig. 5A indicated that the most effective elution performance was achieved using an SDS solution (0.5%, m/m), with a recovery rate of 91.2%. In contrast, the other eluents demonstrated poor elution performance in recovering IgG from the His-rSPG@ZIF-8 composite. It is further demonstrated that the His-rSPG@ZIF-8 composite has a strong specific binding ability to IgG and can only be recovered by changing its spatial structure with a protein denaturant SDS solution. Furthermore, we examined the reusability of the His-rSPG@ZIF-8 composite, which refers to the number of times the nanomaterial can retain its adsorption capacity after successive adsorption and elution cycles of IgG. As shown in Fig. 5B, the adsorption and elution process was repeated for five times and the adsorption efficiency was still above 80%. This demonstrates that the His-rSPG@ZIF-8 composite exhibits

excellent reusability for purifying IgG, making it a promising candidate for repeated applications.

It is possible that the secondary structure of the protein may change during the adsorption and elution of the protein, which may affect the subsequent study of the protein. To investigate whether IgG recovered from the surface of His-rSPG@ZIF-8 composite with SDS solution (0.5%, m/m) as eluent was denatured, circular dichroism (CD) analysis was performed to evaluate the conformational change of IgG (Fig. 4B). Fig. 4Ba shows the water-soluble IgG standard, which exhibits a negative peak at 218 nm, corresponding to the  $\beta$ -fold of IgG. In Fig. 4Bb, the recovered IgG solution after SDS elution exhibited a shift in the peak position, indicating a change in IgG structure during the adsorption and elution process. The observed conformational changes in IgG can be attributed to two potential factors. Firstly, it is possible that the interaction between the His-rSPG@ZIF-8 composite and IgG during the adsorption process induces a conformational change in IgG. Secondly, the eluent SDS itself could also contribute to the conformational alterations in IgG during the elution process. Further studies are required to elucidate the exact mechanisms underlying these conformational changes and to determine the relative contributions of the composite and the eluent in inducing them. In order to determine the cause of the conformational change of IgG, IgG was dissolved in a solution of SDS solution (0.5%, m/m), and the CD spectrum of the solution (Fig. 4Bc) was determined. The peak of the solution was consistent with that of eluted IgG, indicating that SDS was most likely to cause the change. In order to determine whether the conformational change was reversible, SDS was removed by ultrafiltration of the obtained IgG eluate with a 10 kDa ultrafiltration tube and repeated ultrafiltration with secondary water for 5–10 times. CD spectroscopy was performed on the IgG collected after ultrafiltration. As shown in Fig. 4Bd, the peak after ultrafiltration did not completely overlap with the peak of the standard water-soluble IgG. This indicates that after removing SDS, IgG did not fully recover its original secondary structure. Therefore, the structural changes caused by SDS on IgG are irreversible. The reason for this result is that after SDS elution, IgG may undergo aggregation, making it impossible to restore its original structure. This aggregation can be attributed to enhanced protein-protein interactions and non-specific attractive forces. However, the aggregation of proteins can cause changes in the secondary structure, which in turn leads to changes in the CD spectrum. We can maintain the monomeric state of the protein and prevent aggregation by adding protective agents or stabilizers in the subsequent steps.

**Table 1**

Comparisons of the as-prepared His-rSPG@ZIF-8 as adsorbents for the adsorption/extraction of IgG with other solid adsorbents.

| Materials          | Adsorption capacity ( $\text{mg g}^{-1}$ ) | Ref       |
|--------------------|--|-----------|
| Co-MOF-OH          | 97.7                                       | [49]      |
| [PHEMA/PEI]-Cu(II) | 72.28                                      | [50]      |
| PAAm-Alg-ECH-P-Tyr | 91.75                                      | [51]      |
| Mg-Al LDH          | 239  | [52]      |
| His-rSPG@ZIF-8     | 1428.6                                     | this work |

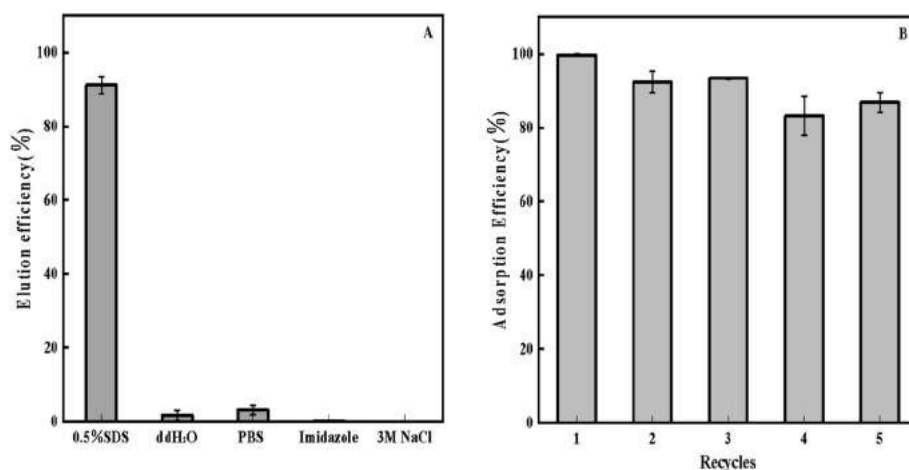


**Fig. 5.** The recovery of the adsorbed IgG from His-rSPG@ZIF-8 by using various stripping reagents (A). His-rSPG@ZIF-8 reproducibility of IgG adsorption performance (B). Protein solution: 100  $\mu\text{g mL}^{-1}$ , 200  $\mu\text{L}$ ; His-rSPG@ZIF-8: 0.05 mg; stripping reagent: 200  $\mu\text{L}$ .

### 3.3. Isolation of IgG from healthy human serum

The feasibility of selective isolation of IgG from complex biological samples by His-rSPG@ZIF-8 composite was investigated using healthy volunteer serum. The specific method was as follows: 0.2 mg His-rSPG@ZIF-8 composite was added to human serum samples diluted 500-fold with a neutral salt concentration of 500  $\text{mmol L}^{-1}$  BR buffer (0.04  $\text{mol L}^{-1}$ , pH 8.0), mixed and shaken for 15 min, centrifuged at 6000 rpm, and the supernatant was retained. The precipitate was pre-washed with ddH<sub>2</sub>O and PBS buffer (0.01  $\text{mol L}^{-1}$ , pH 7.2), and finally the adsorbed protein was recovered with 100  $\mu\text{L}$  of SDS solution (0.5%, m/m) (Scheme S1). The obtained samples were subjected to SDS-PAGE electrophoresis, and the experimental results are shown in Fig. 6. Multiple protein bands (lane 2) were observed in human serum diluted 500 times, mainly Trf (79 kDa), HSA (66.4 kDa), IgG heavy chain (50 kDa), and IgG light chain (25 kDa). After adsorption by the His-rSPG@ZIF-8 composite, it was evident that the IgG heavy and light chain bands in the serum become lighter (lane 3). After elution of the composite with SDS solution (0.5%, m/m), protein bands were observed at 50 kDa and 25 kDa (lane 5), consistent with standard IgG heavy and light chain positions (lane 6). These results indicate that the His-rSPG@ZIF-8 composite can be used as an adsorbent to selectively separate IgG from human serum.

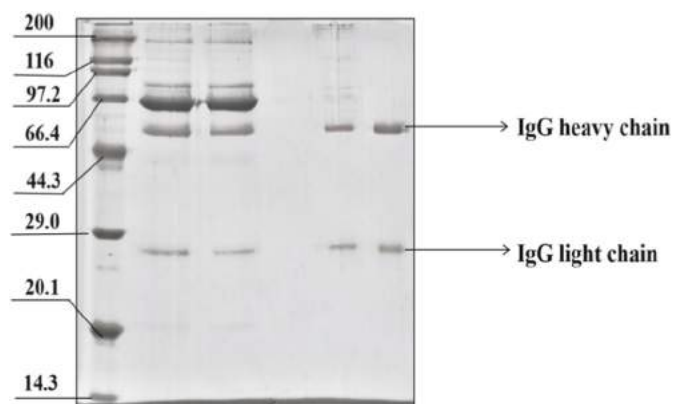


**Fig. 6.** SDS-PAGE assay results. Lane 1: molecular weight standards; Lane 2: 500-fold diluted serum sample; Lane 3: 500-fold diluted serum sample after treating with His-rSPG@ZIF-8 composite; Lane 4: the supernatant obtained after washing the IgG-adsorbed His-rSPG@ZIF-8 composite with PBS buffer (0.01  $\text{mol L}^{-1}$ , pH 7.2); Lane 5: IgG recovered after elution with SDS solution (0.5%, m/m); Lane 6: IgG standard solution (100  $\mu\text{g mL}^{-1}$ ).

To provide further confirmation of the effectiveness of the His-rSPG@ZIF-8 composite for IgG purification and its potential application in proteomics, LC-MS/MS analysis was conducted on serum samples before and after adsorption, as well as after elution with an SDS solution. This analysis aimed to assess the specificity and selectivity of the purification process and to evaluate any potential changes in the protein composition during the purification steps. Fig. 7A lists several proteins that are highly abundant in human serum, such as serum albumin, immunoglobulin light chain (Ig light chain), immunoglobulin heavy chain (Ig heavy chain), apolipoprotein A-I/II, haptoglobin, serotransferrin, alpha-2-macroglobulin, etc. After solid phase extraction with His-rSPG@ZIF-8 composite, it can be seen that the proportion of Ig heavy chain and Ig light chain content decreased from 39.4 % to 30.0 % (Fig. 7B). The results of the supernatant recovered by SDS solution (0.5%, m/m) showed (Fig. 7C) that the content ratio of Ig heavy chain and Ig light chain reached 62.4 %, which proved that the His-rSPG@ZIF-8 composite could achieve enrichment of IgG. Additionally, Fig. 7D provided clear evidence that the serum adsorbed by the composite enabled the identification of 46 low-abundance proteins that were not directly detectable in the original serum sample. A total of 29 proteins were identified from the supernatant recovered by SDS solution (0.5%, m/m), of which 15 proteins were not identified before or after IgG adsorption. It was worth noting that Serpin B4 was also purified to some extent, and the content proportion reaching 9.5 %. This indicates that His-rSPG@ZIF-8 composite exhibited a potential interaction force on Serpin B4. In summary, the two-step extraction process allowed for the identification of a total of 220 proteins, significantly expanding the range and diversity of the identified protein species (Table S2). This underscores the effectiveness of the His-rSPG@ZIF-8 composite in enhancing the proteomic analysis by capturing and identifying a broader range of proteins.

## 4. Conclusions

In this study, we successfully prepared a metal-organic framework composite by modifying it with recombinant protein. The synthesized His-rSPG@ZIF-8 composite underwent thorough characterization through techniques such as FT-IR, Raman, XPS, EDS, BET, SEM, and TEM. The constructed His-rSPG@ZIF-8 composite was then employed for the isolation and purification of IgG. Our findings demonstrated that the His-rSPG@ZIF-8 composite exhibited a high adsorption capacity for IgG under specific conditions. As a result, using this composite as an adsorbent, we successfully developed a novel method for enriching IgG from human serum. Simultaneously, LC-MS/MS analysis of the serum samples revealed the identification of 95 low-abundance proteins

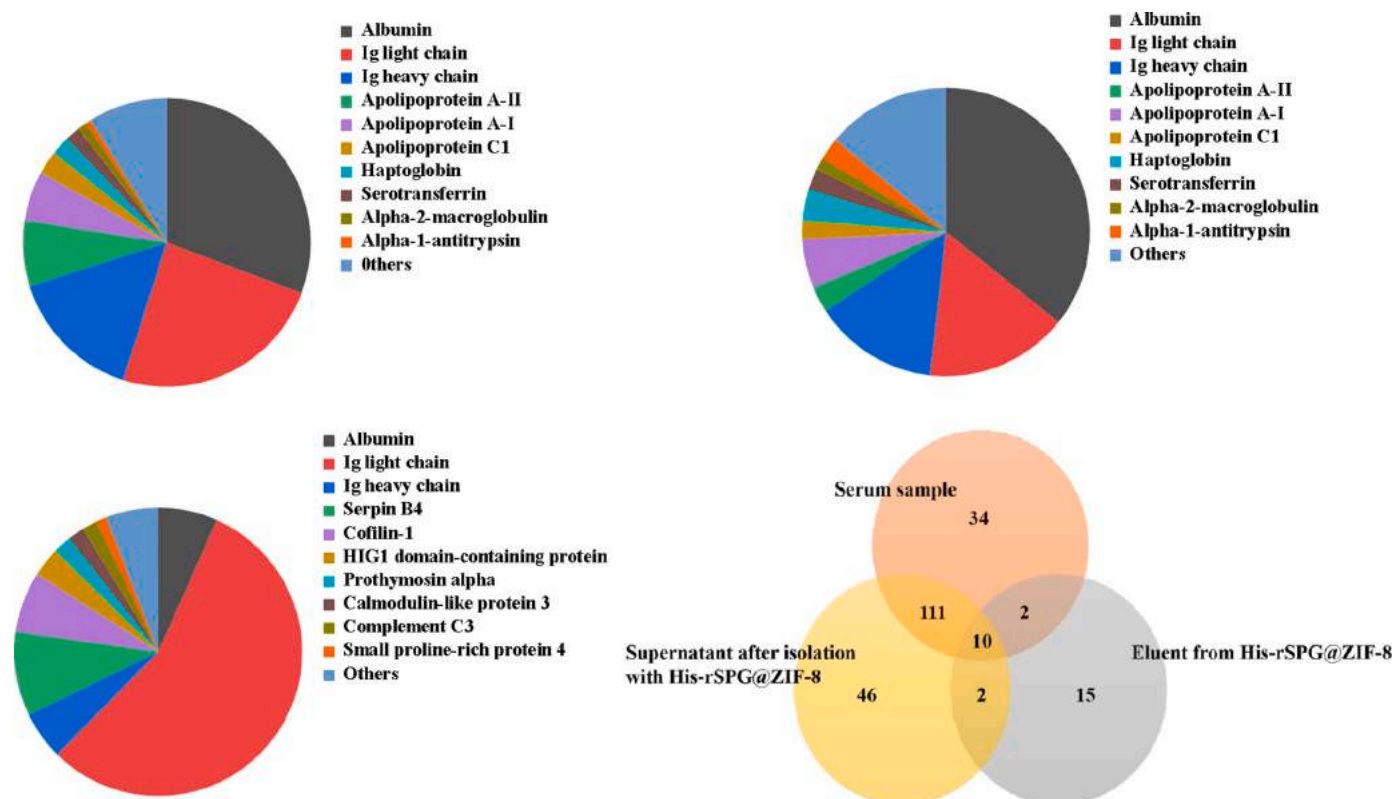


**Fig. 7.** Mass spectrometry data. Distribution of the top 10 most abundant proteins in serum (A), the supernatant after isolation of IgG with His-rSPG@ZIF-8 composite (B) and the recovered solution after SDS removal (C). Venn diagram of the distribution of protein species in human serum, the supernatant after isolation of IgG with His-rSPG@ZIF-8 composite, and the recovered solution after SDS removal (D).

individually. This further emphasizes the potential of our study in expanding the range of identified proteins and highlights the utility of the His-rSPG@ZIF-8 composite in proteomic analyses.

#### CRediT authorship contribution statement

**Yufei Ma:** Writing – original draft, Methodology, Investigation, Formal analysis, Data curation, Conceptualization. **Yuhan Xiang:** Supervision, Methodology, Investigation, Formal analysis, Data curation. **Xin Li:** Validation, Supervision, Resources, Project administration, Funding acquisition. **Dandan Zhang:** Writing – review & editing, Visualization, Validation, Supervision, Software, Resources, Data curation, Conceptualization. **Qing Chen:** Writing – review & editing, Visualization, Validation, Supervision, Resources, Project administration, Methodology, Investigation, Funding acquisition, Conceptualization.

#### Declaration of competing interest

The authors declare that they have no known competing financial interests or personal relationships that could have appeared to influence the work reported in this paper.

#### Data availability

No data was used for the research described in the article.

#### Acknowledgments

The authors appreciate financial supports from the National Natural Science Foundation of China (21804093, 22304123), Natural Science Foundation of Liaoning Province (2023-MS-324, 2023JH/10300079, 2021-BS-284), and Student Research Project of Shenyang Medical

College (20239050).

#### Appendix A. Supplementary data

Supplementary data to this article can be found online at <https://doi.org/10.1016/j.aca.2023.342175>.

#### References

- [1] M. Seifert, R. Küppers, Human memory B cells, *Leukemia* 30 (2016) 2283–2292.
- [2] C.M. Karsten, J. Köhl, The immunoglobulin, IgG Fc receptor and complement triangle in autoimmune diseases, *Immunobiology* 217 (2012) 1067–1079.
- [3] N.A. Pereira, K.F. Chan, P.C. Lin, Z. Song, The “less-is-more” in therapeutic antibodies: afucosylated anti-cancer antibodies with enhanced antibody-dependent cellular cytotoxicity, *mAbs* 10 (2018) 693–711.
- [4] G. Vidarsson, G. Dekkers, T. Rispen, IgG subclasses and allotypes: from structure to effector functions, *Front. Immunol.* 5 (2014) 520.
- [5] R. Labrosse, S. Barmettler, B. Derfalvi, A. Blincoe, G. Cros, J. Lacombe-Barrios, J. Barsalou, N. Yang, N. Alrumayyan, J. Sinclair, M.S. Ong, C.A. Camargo Jr., J. Walter, E. Haddad, Rituximab-induced hypogammaglobulinemia and infection risk in pediatric patients, *J. Allergy Clin. Immunol.* 148 (2021) 148 523–532.
- [6] G. Navarro-Mora, J.J. Alberti, E. Mondou, D. Vilardell, J. Vicente Torres, J. Ayguasanosa, A. Paez, Pharmacokinetic modeling and simulation of subcutaneous and intravenous IgG dosing in patients with primary immunodeficiency diseases, *Int. Immunopharm.* 104 (2022), 108472.
- [7] S. Kdimati, C.S. Mullins, M. Linnebacher, Cancer-Cell-Derived IgG and its potential role in tumor development, *Int. J. Mol. Sci.* 22 (2021), 11597.
- [8] S.L. Lundström, T. Heyder, E. Wiklundh, B. Zhang, A. Eklund, J. Grunewald, R. A. Zubarev, SpotLight proteomics-A IgG-enrichment phenotype profiling approach with clinical implications, *Int. J. Mol. Sci.* 20 (2019) 2157.
- [9] P. Scigalski, P. Kosobucki, Recent materials developed for dispersive solid phase extraction, *Molecules* 25 (2020) 4869.
- [10] J.C. Colmenares, R. Luque, Heterogeneous photocatalytic nanomaterials: prospects and challenges in selective transformations of biomass-derived compounds, *Chem. Soc. Rev.* 43 (2014) 765–778.
- [11] Z. Tavakoli, B. Rasekh, F. Yazdian, A. Maghsoudi, M. Soleimani, J. Mohammadnejad, One-step separation of the recombinant protein by using the amine-functionalized magnetic mesoporous silica nanoparticles; an efficient and facile approach, *Int. J. Biol. Macromol.* 135 (2019) 600–608.

- [12] L. Qian, W. Liu, H. Liu, V. Nica, S. Zhang, Q. Zhou, W. Song, Q. Zhang, Fabrication of raspberry-like cytochrome C surface-imprinted nanoparticles based on MOF composites for high-performance protein separation, *ACS Appl. Mater. Interfaces* 13 (2021) 31010–31020.
- [13] D. Zhu, C. Qin, S. Ao, Q. Su, X. Sun, T. Jiang, K. Pei, H. Ni, P. Ye, Metalloporphyrin-based porous polymers prepared via click chemistry for size-selective adsorption of protein, *J. Biomater. Sci. Polym. Ed.* 29 (2018) 1250–1264.
- [14] T. Khumsap, A. Khumsap, L.T. Nguyen, Epitope-imprinted polymers: applications in protein recognition and separation, *RSC Adv.* 11 (2021), 11403.
- [15] R. Minkner, J. Xu, K. Takemura, J. Boonyakida, H. Wätzig, E.Y. Park, Ni-modified magnetic nanoparticles for affinity purification of His-tagged proteins from the complex matrix of the silkworm fat body, *J. Nanobiotechnol.* 18 (2020) 159.
- [16] Y. Zhen, L. Chen, X. Ma, G. Ding, D. Zhang, Q. Chen,  $\beta$ -Amyloid peptide 1-42-conjugated magnetic nanoparticles for the isolation and purification of glycoproteins in egg white, *ACS Appl. Mater. Interfaces* 13 (2021) 14028–14036.
- [17] P. Dhurjad, C.S. Dharam, N. Ali, N. Kumari, R. Sonti, Metal-organic frameworks in chiral separation of pharmaceuticals, *Chirality* 34 (2022) 1419–1436.
- [18] P.H. Tong, L. Zhu, Y. Zang, J. Li, X.P. He, T.D. James, Metal-organic frameworks (MOFs) as host materials for the enhanced delivery of biomacromolecular therapeutics, *Chem. Commun.* 57 (2021) 12098–12110.
- [19] H. Zhang, L.L. Lou, K. Yu, S. Liu, Advances in chiral metal-organic and covalent organic frameworks for asymmetric catalysis, *Small* 17 (2021), 2005686.
- [20] N.H. Huang, R.T. Li, C. Fan, K.Y. Wu, Z. Zhang, J.X. Chen, Rapid sequential detection of  $Hg^{2+}$  and biothiols by a probe DNA-MOF hybrid sensory system, *J. Inorg. Biochem.* 197 (2019), 110690.
- [21] H. Demir, S. Keskin, Zr-MOFs for CF(4)/CH(4), CH(4)/H(2), and CH(4)/N(2) separation: towards the goal of discovering stable and effective adsorbents, *Mol. Syst. Des. Eng.* 6 (2021) 627–642.
- [22] J. Tao, R. Tan, L. Xu, J. Zhou, Z. Yao, Y. Lei, P. Chen, Z. Li, J.Z. Ou, Ion-Exchange strategy for metal-organic frameworks-derived composites with tunable hollow porous and microwave absorption, *Small Methods* 6 (2022), 2200429.
- [23] K. Yu, T. Wei, Z. Li, J. Li, Z. Wang, Z. Dai, Construction of molecular sensing and logic systems based on site-occupying effect-modulated MOF-DNA interaction, *J. Am. Chem. Soc.* 142 (2020) 21267–21271.
- [24] A. Paul, I.K. Banga, S. Muthukumar, S. Prasad, Engineering the ZIF-8 pore for electrochemical sensor applications-A mini review, *ACS Omega* 7 (2022) 26993–27003.
- [25] M. El Ouardi, A. El Aouni, H. Ait Ahsaine, M. Zbair, A. BaQais, M. Saadi, ZIF-8 metal organic framework composites as hydrogen evolution reaction photocatalyst: a review of the current state, *Chemosphere* 308 (2022), 136483.
- [26] S. Saleem, M.S. Sajid, D. Hussain, B. Fatima, F. Jabeen, M. Najam-Ul-Haq, A. Saed, Highly porous terpolymer-ZIF8@BA MOF composite for identification of mono- and multi-glycosylated peptides/proteins using MS-based bottom-up approach, *Mikrochim. Acta* 187 (2020) 555.
- [27] J. Dhainaut, M. Bonneau, R. Ueoka, K. Kanamori, S. Furukawa, Formulation of metal-organic framework inks for the 3D printing of robust microporous solids toward high-pressure gas storage and separation, *ACS Appl. Mater. Interfaces* 12 (2020) 10983–10992.
- [28] X. Yan, Y. Yao, H. Zhang, J. Xie, C. Xiao, S. Zhang, J. Qi, X. Sun, J. Li, Zeolitic imidazolate framework (ZIF-8)/polyacrylonitrile derived millimeter-sized hierarchical porous carbon beads for peroxymonosulfate catalysis, *Environ. Res.* 206 (2022), 112618.
- [29] Q.X. Wang, Y. Sun, S.F. Li, P.P. Zhang, Q.Q. Yao, Synthesis and Modification of ZIF-8 and its Application in Drug Delivery and Tumor Therapy, *RSC Adv.*, 2020, pp. 37600–37620.
- [30] Y. Ge, K. Wang, J. Liu, Y. Tian, H. Li, H. Wang, Z. Lin, M. Qiu, B. Tang, A ZIF-8-based multifunctional intelligent drug release system for chronic osteomyelitis, *Colloids Surf., B* 212 (2022), 112354.
- [31] G.S. El-Sayyad, O.F. Hasan, A.M. Saad, A.I. El-Batal, Improving the diagnosis of bovine tuberculosis using gold nanoparticles conjugated with purified protein derivative: special regard to staphylococcal protein A and streptococcal protein G, *Environ. Sci. Pollut. Res. Int.* 28 (2021) 29200–29220.
- [32] U. Sjöbring, L. Björck, W. Kastern, Streptococcal protein G. Gene structure and protein binding properties, *J. Biol. Chem.* 266 (1991) 399–405.
- [33] B. Guss, M. Eliasson, A. Olsson, M. Uhlen, A.K. Frej, H. Jornvall, J.I. Flock, M. Lindberg, Structure of the IgG-binding regions of streptococcal protein G, *EMBO J.* 5 (1986) 1567–1575.
- [34] C.R. Goward, J.P. Murphy, T. Atkinson, D.A. Barstow, Expression and purification of a truncated recombinant streptococcal Protein G, *Biochem. J.* 267 (1990) 171–177.
- [35] B. Akerström, T. Brodin, K. Reis, L. Björck, Protein G: a powerful tool for binding and detection of monoclonal and polyclonal antibodies, *J. Immunol.* 135 (1985) 2589, 1592.
- [36] E. Darcy, P. Leonard, J. Fitzgerald, M. Danaher, H. Ma, Richard O' Kennedy, Purification of antibodies using affinity chromatography, *Methods Mol. Biol.* 1485 (2017) 305–318.
- [37] J. Zheng, Z. Lin, G. Lin, H. Yang, L. Zhang, Preparation of magnetic metal-organic framework nanocomposites for highly specific separation of histidine-rich proteins, *J. Mater. Chem. B* 3 (2015) 2185–2191.
- [38] B. Niu, Z. Zhai, J. Wang, C. Li, Preparation of ZIF-8/PAN composite nanofiber membrane and its application in acetone gas monitoring, *Nanotechnology* 34 (2023), 245710.
- [39] X. Niu, S. Yan, L. Wang, J. Chen, R. Zhao, H. Li, J. Liu, K. Wang, Induction of chiral polymers from metal-organic framework for stereoselective recognition, *Anal. Chim. Acta* 1196 (2022), 339546.
- [40] P.H. Chang, C.Y. Chen, R. Mukhopadhyay, W. Chen, Y.M. Tzou, B. Sarkar, Novel MOF-808 metal-organic framework as highly efficient adsorbent of perfluorooctane sulfonate in water, *J. Colloid Interface Sci.* 623 (2022) 627–636.
- [41] J. Liu, B. Li, Y.Q. Li, W.J. Zheng, 1-(2-(4-Dichloro-benzyl-idene)amino)eth-yl)-3-methyl-imidazolium hexa-fluoro-phosphate, *Acta Crystallogr., Sect. E: Struct. Rep. Online* 65 (2009), o2972.
- [42] G. Kumari, K. Jayaramulu, T.K. Maji, C. Narayana, Temperature induced structural transformations and gas adsorption in the zeolitic imidazolate framework ZIF-8: a Raman study, *J. Phys. Chem. A* 117 (2013) 11006–11012.
- [43] T. Luczak, M. Bettowska-Brzezinska, M. Bron, R. Holze, The adsorption of benzylamine on a polycrystalline gold electrode: a combined spectroelectrochemical study, *Vib. Spectrosc.* 15 (1997) 17–25.
- [44] M. Anisi, A.A. Ghoreyshi, E. Mehrvarz, A. Rahimpour, Synthesize optimization, characterization, and application of ZIF-8 adsorbent for elimination of olive oil from aqueous solution, *Environ. Sci. Pollut. Res. Int.* 28 (2021) 12725–12739.
- [45] W. He, H. Huang, J. He, S. Subhan, Y. Peng, M. Huang, H. He, Y. Tang, Z. Zhao, Amino acids imprinted ZIF-8s for the highly efficient and selective adsorption of antioxidant peptides from silkworm pupa protein, *Food Res. Int.* 157 (2022), 111406.
- [46] C.H. Li, W.X. Yang, X.S. Zhang, Y. Han, W.Z. Tang, T.L. Yue, Z.H. Li, A 3D hierarchical dual-metal-organic framework heterostructure up-regulating the pre-concentration effect for ultrasensitive fluorescence detection of tetracycline antibiotics, *J. Mater. Chem. C* 8 (2020) 2054–2064.
- [47] H.G. Lee, S. Kang, J.S. Lee, Binding characteristics of staphylococcal protein A and streptococcal protein G for fragment crystallizable portion of human immunoglobulin G, *Comput. Struct. Biotechnol. J.* 19 (2021) 3372–3383.
- [48] R.K. Jha, T. Gaiotto, A.R. Bradbury, C.E. Strauss, An improved Protein G with higher affinity for human/rabbit IgG Fc domains exploiting a computationally designed polar network, *Protein Eng. Des. Sel.* 27 (2014) 127–134.
- [49] Z. Hu, J. Meng, X. Wang, W. Li, X. Chen, Tailoring the surface properties of Co-based metal-organic frameworks for highly efficient and selective enrichment of immunoglobulin G, *ACS Appl. Mater. Interfaces* 12 (2020) 55453–55459.
- [50] M. Bakhshpour, A. Derazshamshir, N. Bereli, A. Elkak, A. Denizli, [PHEMA/PEI]-Cu(II) based immobilized metal affinity chromatography cryogels: application on the separation of IgG from human plasma, *Mater. Sci. Eng., C* 61 (2016) 824–831.
- [51] C. Marcuz, C. Alves Mourao, K. Haupt, S.M. Alves Bueno, Performance of phospho-L-tyrosine immobilized onto alginate/polyacrylamide-based cryogels: effect of ligand coupling on human IgG adsorption and Fab fragments separation, *J. Chromatogr. B* 1165 (2021), 122530.
- [52] D.R. Gondim, J.A. Cecilia, S.O. Santos, T.N.B. Rodrigues, J.E. Aguiar, E. Vilarrasa-Garcia, E. Rodriguez-Castellon, D.C.S. Azevedo, I.J. Silva Jr., Influence of buffer solutions in the adsorption of human serum proteins onto layered double hydroxide, *Int. J. Biol. Macromol.* 106 (2018) 396–409.